

Role of crystal-field-splitting and long-range-hoppings on superconducting pairing symmetry of $\text{La}_3\text{Ni}_2\text{O}_7$

Hongquan Liu^{1,2*}, Chengliang Xia^{1*}, Shengjie Zhou¹ and Hanghui Chen^{1,3†}

¹*NYU-ECNU Institute of Physics, NYU Shanghai, Shanghai 200122, China*

²*Department of Physics, Brown University,*

182 Hope Street, Providence, RI 02912, USA

³*Department of Physics, New York University, New York, New York 10012, USA*

(Dated: November 14, 2023)

Abstract

We study the bilayer two-orbital model for superconducting pairing symmetry of $\text{La}_3\text{Ni}_2\text{O}_7$ under pressure. By combining density-functional-theory (DFT), maximally-localized-Wannier-function, and linearized Eliashberg equation with random-phase-approximation, we find that the superconducting pairing symmetry of $\text{La}_3\text{Ni}_2\text{O}_7$ is robustly d_{xy} if its DFT band structure is accurately reproduced in the downfolded model. We further show that fine-tuning of crystal-field-splitting between two Ni- e_g orbitals qualitatively affects superconducting pairing symmetry of the bilayer two-orbital model, which changes from d_{xy} to s_{\pm} as the crystal-field-splitting exceeds a critical value. When the model only includes nearest-neighbor and second-nearest-neighbor hoppings, the crystal-field-splitting obtained by fitting to the DFT band structure is larger than the critical value and thus leads to s_{\pm} superconducting pairing symmetry. When all nonzero long-range-hoppings are also included in the model, the fitted crystal-field-splitting is reduced and smaller than the critical value, which makes d_{xy} superconducting pairing symmetry more favorable than s_{\pm} symmetry. Our work demonstrates that in downfolded effective models, the details of band structure can play a crucial role in determining pairing symmetry in multi-orbital unconventional superconductors (such as $\text{La}_3\text{Ni}_2\text{O}_7$).

* These authors contributed equally to this work.

† hanghui.chen@nyu.edu

The recent discovery of superconductivity in $\text{La}_3\text{Ni}_2\text{O}_7$ under pressure has drawn great attention [1–38]. It not only adds a new member to the family of nickelate superconductors [39–47], but also substantially increases the transition temperature to near 80 K [1]. A bilayer two-orbital model that consists of Ni- e_g orbitals has been widely used as the minimum model to study $\text{La}_3\text{Ni}_2\text{O}_7$ under pressure [5–11]. The prototype is from Ref. [5] (referred to as Luo’s model in this work). Based on the bilayer two-orbital model, a number of studies use different many-body techniques and find that the leading superconducting instability of $\text{La}_3\text{Ni}_2\text{O}_7$ has s_{\pm} pairing symmetry [5–11], distinct from the pairing symmetry of well-known cuprate superconductors [48–50] but reminiscent of iron-based superconductors [51–53]. On the other hand, Ref. [36] finds d -wave pairing symmetry using the same effective model and weak-coupling theory calculations.

In this work, we combine density-functional-theory (DFT) [54, 55], maximally-localized-Wannier-function (MLWF) [56, 57], and linearized Eliashberg equation with random-phase-approximation (RPA) [58–62] to study the bilayer two-orbital model for superconducting pairing symmetry of $\text{La}_3\text{Ni}_2\text{O}_7$. We find that if the downfolded model accurately reproduces the DFT band structure of $\text{La}_3\text{Ni}_2\text{O}_7$, the leading superconducting instability has a robust d_{xy} symmetry. We refer to the bilayer two-orbital model with this type of “exact” downfolding as Wannier’s model. We further show that in both Luo’s and Wannier’s models, fine-tuning of crystal-field-splitting between two Ni- e_g orbitals qualitatively affects superconducting pairing symmetry, which changes from d_{xy} to s_{\pm} when the crystal-field-splitting exceeds a critical value. In Luo’s model which only includes nearest-neighbor and second-nearest-neighbor hoppings, its crystal-field-splitting obtained from fitting to the DFT band structure of $\text{La}_3\text{Ni}_2\text{O}_7$ is larger than the critical value, thereby leading to a s_{\pm} superconducting pairing symmetry. By contrast, in Wannier’s model in which all nonzero long-range-hoppings are also included, its crystal-field-splitting obtained from Wannier fitting is reduced and substantially smaller than the critical value. Thus the pairing symmetry of leading superconducting instability in Wannier’s model is robustly d_{xy} . Our work highlights the sensitivity of superconducting pairing symmetry to the details of band structure in the bilayer two-orbital model when it is applied to study $\text{La}_3\text{Ni}_2\text{O}_7$ under pressure.

We perform DFT calculations, as implemented in the Vienna ab initio simulation package (VASP) [63, 64]. We use the MLWF to do the downfolding from DFT band structure [65] and obtain a bilayer two-orbital model for linearized Eliashberg equation calculations. We use

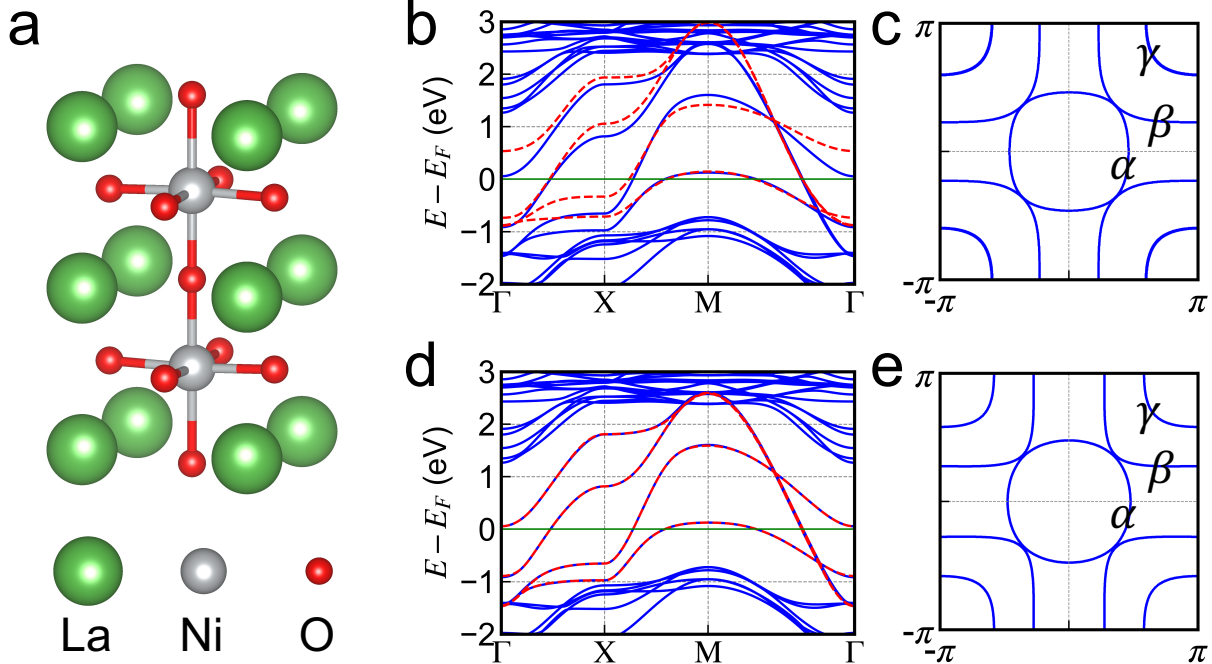


FIG. 1: (a) Crystal structure of $\text{La}_3\text{Ni}_2\text{O}_7$ under high pressure. (b) Comparison of DFT band structure of $\text{La}_3\text{Ni}_2\text{O}_7$ under 30 GPa (blue solid curves) to the band structure of Luo's model (red dashed curves). (c) The Fermi surface of Luo's model. (d) Comparison of DFT band structure of $\text{La}_3\text{Ni}_2\text{O}_7$ under 30 GPa (blue solid curves) to the band structure of Wannier's model (red dashed curves). (e) The Fermi surface of Wannier's model.

RPA to treat the local Hubbard interaction on Ni- e_g orbitals and obtain the effective pairing potential. The basis of the bilayer two-orbital model in this study is: (Ni1- $d_{3z^2-r^2}$, Ni1- $d_{x^2-y^2}$, Ni2- $d_{3z^2-r^2}$, Ni2- $d_{x^2-y^2}$). The dispersion parameters of Luo's model and Wannier's model, the details of DFT, RPA and linearized Eliashberg equation calculations, as well as other computational specifics are found in the Supplementary Materials.

Fig. 1(a) shows the crystal structure of $\text{La}_3\text{Ni}_2\text{O}_7$ under high pressure. In DFT calculations, we find that after atomic relaxation, $\text{La}_3\text{Ni}_2\text{O}_7$ under 30 GPa crystallizes in a $Fmmm$ structure (space group no.69), consistent with the experiment [1]. However, the in-plane lattice constants a and b are very close, almost leading to a C_4 symmetry about z axis [13]. Following the previous studies [5–11], because the inter-block interaction is weak, we focus on one-block of $\text{La}_3\text{Ni}_2\text{O}_7$, whose DFT band structure is used to do the downfolding to a bilayer two-orbital model. Fig. 1(b) shows the comparison of DFT band structure of $\text{La}_3\text{Ni}_2\text{O}_7$

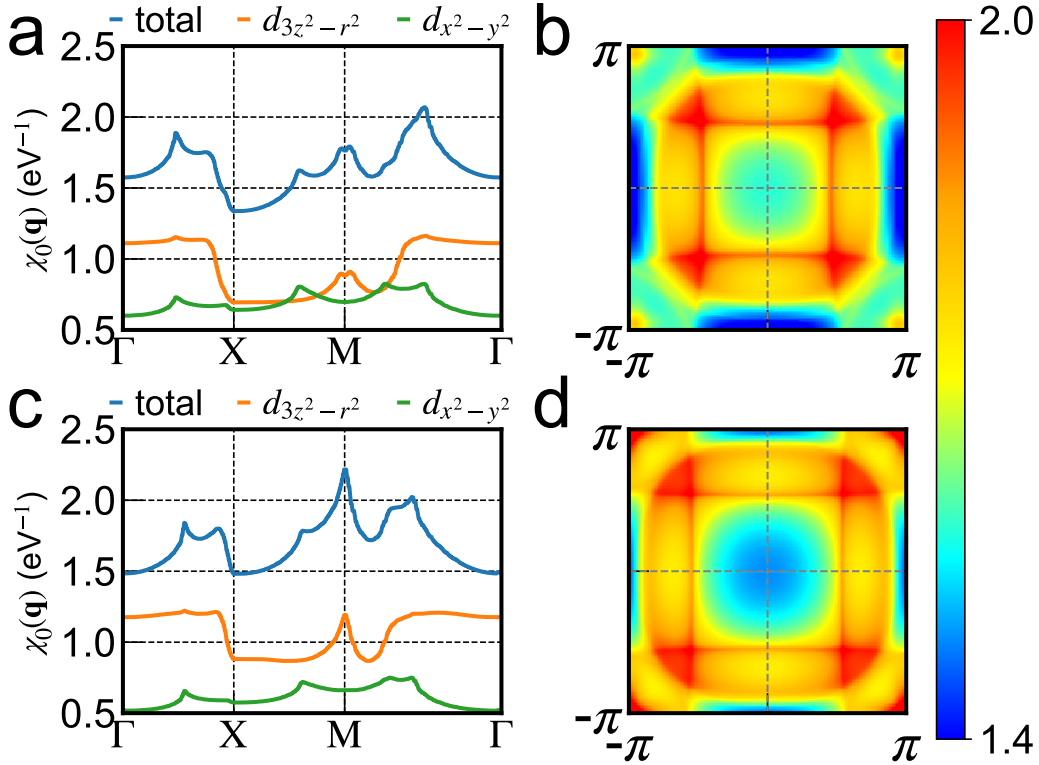


FIG. 2: Bare susceptibility $\chi_0(\mathbf{q})$ at $T = 116$ K. (a) Total and orbital-projected $\chi_0(\mathbf{q})$ of Luo's model along the high-symmetry \mathbf{q} -path. (b) Total $\chi_0(\mathbf{q})$ of Luo's model in the 2D Brillouin zone. (c) Total and orbital-projected $\chi_0(\mathbf{q})$ of Wannier's model along the high-symmetry \mathbf{q} -path. (d) Total $\chi_0(\mathbf{q})$ of Wannier's model in the 2D Brillouin zone.

to the band structure of Luo's model, which reasonably reproduces the four Ni- e_g -derived bands around the Fermi level. Fig. 1(c) shows the Fermi surface of Luo's model, which has three sheets in the two-dimensional (2D) Brillouin zone, labeled as α , β and γ . Fig. 1(d) shows the comparison of DFT band structure of $\text{La}_3\text{Ni}_2\text{O}_7$ and the band structure from Wannier's model. By additionally including all nonzero long-range-hoppings, Wannier's model exactly reproduces the four Ni- e_g -derived bands. The resulting Fermi surface also has three sheets, which is very similar to that of Luo's model, as shown in Fig. 1(e). However, as we show below, the two seemingly identical Fermi surfaces have different pairing symmetries of leading superconducting instability.

Next we compare total and orbital-projected bare susceptibility $\chi_0(\mathbf{q})$ of the two models (the definition of different kinds of susceptibility is found in the Supplementary Materials).

Fig. 2(a) and (b) show $\chi_0(\mathbf{q})$ of Luo’s model on a high-symmetry \mathbf{q} -path and in the 2D Brillouin zone. In panel (a), both total and orbital-projected $\chi_0(\mathbf{q})$ are shown, while in panel (b), we only show total $\chi_0(\mathbf{q})$. In Luo’s model, Ni- $d_{3z^2-r^2}$ orbital overall has a larger susceptibility than Ni- $d_{x^2-y^2}$ orbital. The highest peak value of total $\chi_0(\mathbf{q})$ is along Γ to M , close to $(\frac{\pi}{2}, \frac{\pi}{2})$. This peak value would be substantially enhanced when local Hubbard interactions are added on Ni orbitals in RPA calculations (see the Supplementary Materials). Then we perform the same calculations on Wannier’s model and show the results in Fig. 2(c) and (d). We find that while $\chi_0(\mathbf{q})$ of Wannier’s model is qualitatively similar to that of Luo’s model, there are some notable differences. In Wannier’s model, the $d_{3z^2-r^2}$ -projected $\chi_0(\mathbf{q})$ is increased, in particular at M point. This suggests that d -wave pairing might be favored in Wannier’s model.

Now we study superconducting pairing symmetry of the two models, which have qualitative differences, despite the fact that the two models have very similar band structure and Fermi surface. We use linearized Eliashberg equation with RPA method to treat the local Hubbard interaction for the effective pairing potential. In Fig. 3(a), we show the superconducting pairing symmetry of Luo’s model. We find that the first three leading superconducting instabilities have s_{\pm} , d_{xy} , and $d_{x^2-y^2}$ pairing symmetries, respectively. This result does not change as interaction strength U varies in a reasonable range. Fig. 3(b) shows the gap function for the leading eigenvalue of linearized Eliashberg equation, using Luo’s model. In this gap function, α and γ sheets are of the same sign, while β sheet is of the opposite sign, which is consistent with the previous studies [7–10]. In Fig. 3(c), we show the superconducting pairing symmetry of Wannier’s model. By contrast, we find that the first three leading superconducting instabilities have d_{xy} , $d_{x^2-y^2}$, and s_{\pm} pairing symmetries, respectively. This result is qualitatively different from Luo’s model and does not change with interaction strength, either. Fig. 3(d) shows the gap function for the leading eigenvalue of linearized Eliashberg equation, using Wannier’s model. This gap function clearly exhibits d_{xy} symmetry, consistent with Ref. [36].

To reveal the key difference between the two models and what is the control parameter for superconducting pairing symmetry, we perform a “thought-experiment”. For each model, we manually change the onsite energy difference Δ between Ni- $d_{3z^2-r^2}$ and Ni- $d_{x^2-y^2}$ orbitals, which is a measure of crystal-field-splitting between the two Ni- e_g orbitals. For a given value of Δ , we re-calculate the band structure and the superconducting pairing symmetry using

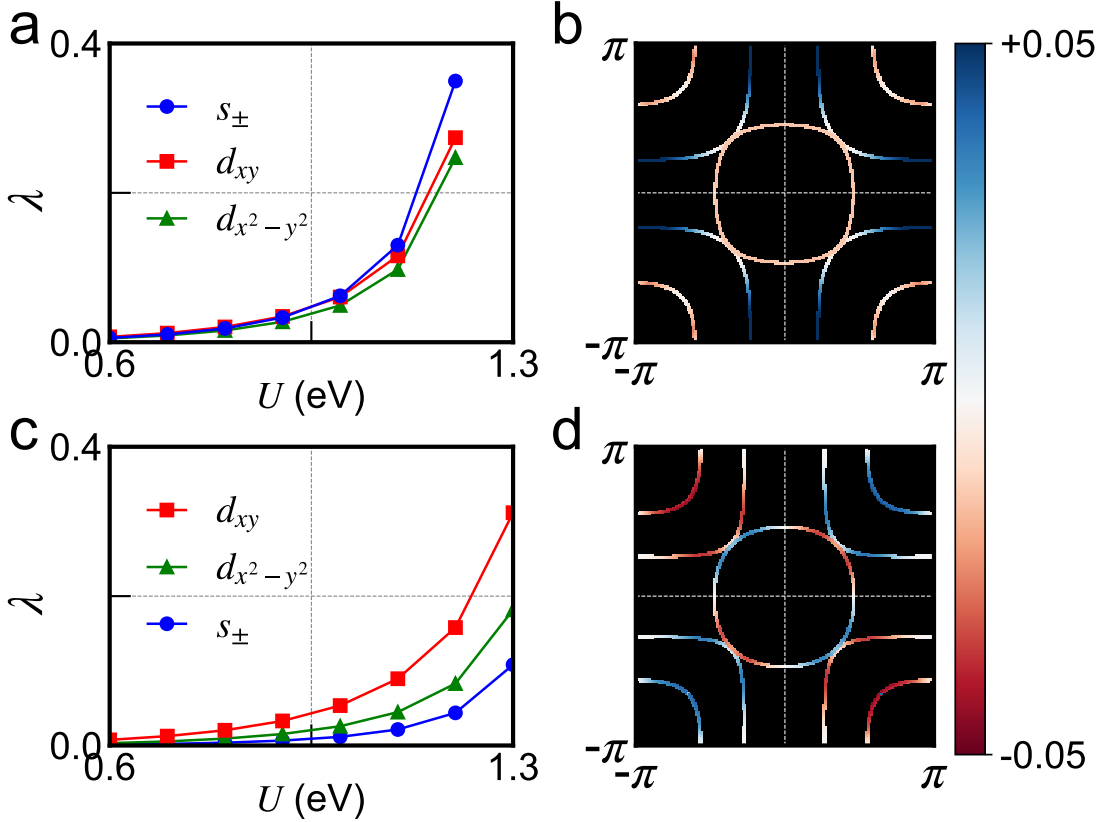


FIG. 3: (a) The eigenvalues λ of linearized Eliashberg's equation with RPA method, using Luo's model. The first three leading superconducting instabilities have s_{\pm} (blue circles), d_{xy} (red squares), and $d_{x^2-y^2}$ (green triangles) symmetries, respectively. (b) Gap function for the leading superconducting instability of Luo's model calculated at $U = 1.2$ eV and $J = 0.15U = 0.18$ eV, which exhibits s_{\pm} symmetry. (c) The eigenvalues λ of linearized Eliashberg's equation with RPA method, using Wannier's model. The first three leading superconducting instabilities have d_{xy} (red squares), $d_{x^2-y^2}$ (green triangles), and s_{\pm} (blue circles) symmetries, respectively. (d) Gap function for the leading superconducting instability of Wannier's model calculated at $U = 1.2$ eV and $J = 0.15U = 0.18$ eV, which exhibits d_{xy} symmetry.

linearized Eliashberg equation with RPA method. We use $U = 1.2$ eV and $J = 0.15U = 0.18$ eV. The following results do not qualitatively change if the interaction strength takes other reasonable values (see the Supplementary Materials). In Fig. 4(a), we compare the band structure of Luo's model to the DFT band structure of $\text{La}_3\text{Ni}_2\text{O}_7$ under 30 GPa, as Δ is fine-tuned in a small range from 0.20 eV to 0.40 eV. The optimal value of Δ in Luo's model

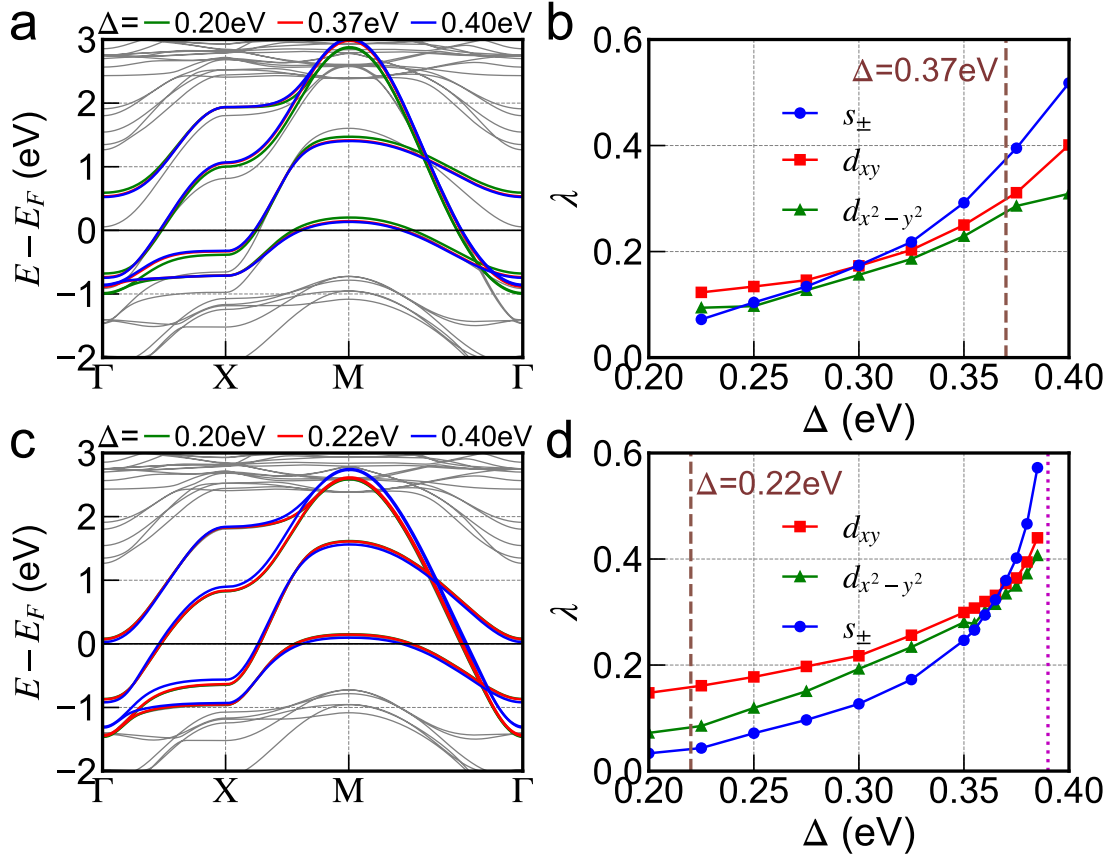


FIG. 4: (a) Comparison of DFT band structure of $\text{La}_3\text{Ni}_2\text{O}_7$ under 30 GPa (gray) to the band structure of Luo's model at a few different crystal-field-splitting Δ . (b) The eigenvalues λ of linearized Eliashberg equation with RPA method for the first three superconducting instabilities in Luo's model, calculated at $U = 1.2$ eV and $J = 0.15U = 0.18$ eV. The leading superconducting pairing symmetry is d_{xy} (s_{\pm}) when Δ is smaller (larger) than 0.30 eV. The dashed brown line highlights the optimal value of $\Delta = 0.37$ eV in the original Luo's model. (c) Comparison of DFT band structure of $\text{La}_3\text{Ni}_2\text{O}_7$ under 30 GPa (gray) to the band structure of Wannier's model at a few different crystal-field-splitting Δ . (d) The eigenvalues λ of linearized Eliashberg equation with RPA method for the first three superconducting instability in Wannier's model. The leading superconducting pairing symmetry is d_{xy} (s_{\pm}) when Δ is smaller (larger) than 0.37 eV. The dashed brown line highlights the optimal value of $\Delta = 0.22$ eV in the original Wannier's model. The purple dotted line shows that spin-density-wave instability occurs at this value of Δ in the RPA calculations.

is 0.37 eV, based on the fitting. We find that tuning Δ in this small range yields marginal

effects on the overall band structure, since the total bandwidth is about 4 eV. In Fig. 4(b), we show the eigenvalues for the first three leading superconducting instabilities, using Luo’s model, as Δ varies. We find that the leading superconducting instability has d_{xy} symmetry (s_{\pm} symmetry) if Δ is smaller (larger) than 0.30 eV. The brown dashed line highlights the optimal value of Δ in Luo’s model, at which the leading superconducting pairing symmetry is s_{\pm} , consistent with the previous studies [5–11]. In Fig. 4(c), we compare the band structure of Wannier’s model to the DFT band structure of $\text{La}_3\text{Ni}_2\text{O}_7$ under 30 GPa, as Δ is fine-tuned in the same range. The optimal value of Δ in Wannier’s model is 0.22 eV, smaller than that in Luo’s model due to the inclusion of all nonzero long-range-hoppings. Similar to Luo’s model, we find insignificant changes in the band structure of Wannier’s model by such fine-tuning of Δ . Then we re-calculate the superconducting pairing symmetry at the same U and J values, using Wannier’s model, as Δ varies. Fig. 4(d) shows the eigenvalues for the three leading superconducting instabilities. We find a similar trend that a smaller (larger) Δ favors d_{xy} symmetry (s_{\pm} symmetry) with the critical point at 0.37 eV. The dashed brown line highlights the optimal value of Δ in Wannier’s model, which is substantially smaller than the critical value. Thus the leading superconducting pairing symmetry of Wannier’s model is d_{xy} , consistent with Ref. [36]. In passing, we mention that when the crystal-field-splitting Δ of Wannier’s model is 0.39 eV (purple dotted line in panel (d)), spin-density-wave instability occurs in the RPA calculations.

Experimentally it is challenging to directly probe superconducting pairing symmetry in $\text{La}_3\text{Ni}_2\text{O}_7$ because so far $\text{La}_3\text{Ni}_2\text{O}_7$ only exhibits superconductivity under pressure [1]. The take-home message from this study is that superconducting pairing symmetry of $\text{La}_3\text{Ni}_2\text{O}_7$ is very sensitive to the details of band structure in downfolded models, such as crystal-field-splitting and long-range-hoppings. A small increase in Ni- e_g crystal-field-splitting qualitatively changes the superconducting pairing symmetry of the bilayer two-orbital model from d_{xy} to s_{\pm} , even though the modification to band structure and Fermi surface is marginal. When the model only includes short-range-hoppings up to second-nearest-neighbors, the resulting crystal-field-splitting from fitting to DFT band structure of $\text{La}_3\text{Ni}_2\text{O}_7$ is larger than the critical value, which stabilizes s_{\pm} superconducting pairing symmetry. When the model includes all nonzero hoppings, which exactly reproduces the DFT band structure of $\text{La}_3\text{Ni}_2\text{O}_7$, the crystal-field-splitting obtained from the Wannier fitting gets reduced and is substantially smaller than the critical value. This leads to a robust d_{xy} superconducting

pairing symmetry in RPA calculations. We conjecture that such sensitivity of superconducting pairing symmetry to band structure may exist in other multi-orbital unconventional superconductors and thus care is needed in the downfolding procedure when studying unconventional superconductivity in realistic materials.

Acknowledgments

We are grateful to Xianxin Wu, Yi-feng Yang and Dao-Xin Yao for useful discussions. This project was financially supported by the National Key R&D Program of China under project number 2021YFE0107900, and Science and Technology Commission of Shanghai Municipality under grant number 23ZR1445400. NYU High-Performance-Computing (HPC) provides computational resources.

-
- [1] H. Sun, M. Huo, X. Hu, J. Li, Z. Liu, Y. Han, L. Tang, Z. Mao, P. Yang, B. Wang, et al., *Nature* **621**, 493 (2023).
 - [2] J. Hou, P.-T. Yang, Z.-Y. Liu, J.-Y. Li, P.-F. Shan, L. Ma, G. Wang, N.-N. Wang, H.-Z. Guo, J.-P. Sun, et al., *Chinese Physics Letters* **40**, 117302 (2023).
 - [3] Q. Qin and Y.-f. Yang, *Phys. Rev. B* **108**, L140504 (2023).
 - [4] D. A. Shilenko and I. V. Leonov, *Phys. Rev. B* **108**, 125105 (2023).
 - [5] Z. Luo, X. Hu, M. Wang, W. Wú, and D.-X. Yao, *Phys. Rev. Lett.* **131**, 126001 (2023).
 - [6] J. Huang, Z. D. Wang, and T. Zhou, *Phys. Rev. B* **108**, 174501 (2023).
 - [7] Y. Zhang, L.-F. Lin, A. Moreo, T. A. Maier, and E. Dagotto, *Phys. Rev. B* **108**, 165141 (2023).
 - [8] Q.-G. Yang, D. Wang, and Q.-H. Wang, *Phys. Rev. B* **108**, L140505 (2023).
 - [9] Y. Gu, C. Le, Z. Yang, X. Wu, and J. Hu, arXiv:2306.07275 (2023).
 - [10] Y. Zhang, L.-F. Lin, A. Moreo, T. A. Maier, and E. Dagotto, arXiv:2307.15276 (2023).
 - [11] Z. Luo, B. Lv, M. Wang, W. Wú, and D.-X. Yao, arXiv:2308.16564 (2023).
 - [12] H. Oh and Y.-H. Zhang, arXiv:2307.15706 (2023).
 - [13] B. Geisler, J. J. Hamlin, G. R. Stewart, R. G. Hennig, and P. J. Hirschfeld, arXiv:2309.15078 (2023).

- [14] H. Lange, L. Homeier, E. Demler, U. Schollwöck, F. Grusdt, and A. Bohrdt, arXiv:2309.15843 (2023).
- [15] H. LaBollita, V. Pardo, M. R. Norman, and A. S. Botana, arXiv:2309.17279 (2023).
- [16] Y. Zhang, D. Su, Y. Huang, H. Sun, M. Huo, Z. Shan, K. Ye, Z. Yang, R. Li, M. Smidman, et al., arXiv:2307.14819 (2023).
- [17] J. Yang, H. Sun, X. Hu, Y. Xie, T. Miao, H. Luo, H. Chen, B. Liang, W. Zhu, G. Qu, et al., arXiv:2309.01148 (2023).
- [18] Z. Pan, C. Lu, F. Yang, and C. Wu, arXiv:2309.06173 (2023).
- [19] Y.-H. Tian, Y. Chen, J.-M. Wang, R.-Q. He, and Z.-Y. Lu, arXiv:2308.09698 (2023).
- [20] Y. Zhang, L.-F. Lin, A. Moreo, T. A. Maier, and E. Dagotto, arXiv:2310.17871 (2023).
- [21] S. Ryee, N. Witt, and T. O. Wehling, arXiv:2310.17465 (2023).
- [22] C. Lu, Z. Pan, F. Yang, and C. Wu, arXiv:2310.02915 (2023).
- [23] K. Jiang, Z. Wang, and F.-C. Zhang, arXiv:2308.06771 (2023).
- [24] G. Wang, N. Wang, J. Hou, L. Ma, L. Shi, Z. Ren, Y. Gu, X. Shen, H. Ma, P. Yang, et al., arXiv:2309.17378 (2023).
- [25] H. Yang, H. Oh, and Y.-H. Zhang, arXiv:2309.15095 (2023).
- [26] T. Kaneko, H. Sakakibara, M. Ochi, and K. Kuroki, arXiv:2310.01952 (2023).
- [27] Z. Liao, L. Chen, G. Duan, Y. Wang, C. Liu, R. Yu, and Q. Si, arXiv:2307.16697 (2023).
- [28] L. C. Rhodes and P. Wahl, arXiv:2309.15745 (2023).
- [29] J.-X. Zhang, H.-K. Zhang, Y.-Z. You, and Z.-Y. Weng, arXiv:2309.05726 (2023).
- [30] X.-Z. Qu, D.-W. Qu, J. Chen, C. Wu, F. Yang, W. Li, and G. Su, arXiv:2307.16873 (2023).
- [31] C. Lu, Z. Pan, F. Yang, and C. Wu, arXiv:2307.14965 (2023).
- [32] X. Chen, P. Jiang, J. Li, Z. Zhong, and Y. Lu, arXiv:2307.07154 (2023).
- [33] Y. Cao and Y. feng Yang, arXiv:2307.06806 (2023).
- [34] V. Christiansson, F. Petocchi, and P. Werner, arXiv:2306.07931 (2023).
- [35] Y. Shen, M. Qin, and G.-M. Zhang, arXiv:2306.07837 (2023).
- [36] F. Lechermann, J. Gondolf, S. Bötzel, and I. M. Eremin, arXiv:2306.05121 (2023).
- [37] Q. Li, Y.-J. Zhang, Z.-N. Xiang, Y. Zhang, X. Zhu, and H.-H. Wen, arXiv:2311.05453 (2023).
- [38] J. Chen, F. Yang, and W. Li, arXiv:2311.05491 (2023).
- [39] D. Li, K. Lee, B. Y. Wang, M. Osada, S. Crossley, H. R. Lee, Y. Cui, Y. Hikita, and H. Y. Hwang, *Nature* **572**, 624 (2019).

- [40] D. Li, B. Y. Wang, K. Lee, S. P. Harvey, M. Osada, B. H. Goodge, L. F. Kourkoutis, and H. Y. Hwang, *Phys. Rev. Lett.* **125**, 027001 (2020).
- [41] S. Zeng, C. S. Tang, X. Yin, C. Li, M. Li, Z. Huang, J. Hu, W. Liu, G. J. Omar, H. Jani, et al., *Phys. Rev. Lett.* **125**, 147003 (2020).
- [42] Q. Gu, Y. Li, S. Wan, H. Li, W. Guo, H. Yang, Q. Li, X. Zhu, X. Pan, Y. Nie, et al., *Nat Commun* **11**, 6027 (2020).
- [43] Y. Gu, S. Zhu, X. Wang, J. Hu, and H. Chen, *Commun Phys* **3**, 84 (2020).
- [44] S. Zeng, C. Li, L. E. Chow, Y. Cao, Z. Zhang, C. S. Tang, X. Yin, Z. S. Lim, J. Hu, P. Yang, et al., *Science Advances* **8**, eabl9927 (2022).
- [45] M. Osada, B. Y. Wang, B. H. Goodge, S. P. Harvey, K. Lee, D. Li, L. F. Kourkoutis, and H. Y. Hwang, *Advanced Materials* **33**, 2104083 (2021).
- [46] C. Xia, J. Wu, Y. Chen, and H. Chen, *Phys. Rev. B* **105**, 115134 (2022).
- [47] H. Chen, Y.-f. Yang, G.-M. Zhang, and H. Liu, *Nat Commun* **14**, 5477 (2023).
- [48] D. J. Van Harlingen, *Rev. Mod. Phys.* **67**, 515 (1995).
- [49] C. C. Tsuei and J. R. Kirtley, *Rev. Mod. Phys.* **72**, 969 (2000).
- [50] L. Taillefer, *Annual Review of Condensed Matter Physics* **1**, 51 (2010).
- [51] A. V. Chubukov, D. V. Efremov, and I. Eremin, *Phys. Rev. B* **78**, 134512 (2008).
- [52] P. J. Hirschfeld, M. M. Korshunov, and I. I. Mazin, *Reports on Progress in Physics* **74**, 124508 (2011).
- [53] G. R. Stewart, *Rev. Mod. Phys.* **83**, 1589 (2011).
- [54] P. Hohenberg and W. Kohn, *Phys. Rev.* **136**, B864 (1964).
- [55] W. Kohn and L. J. Sham, *Phys. Rev.* **140**, A1133 (1965).
- [56] N. Marzari, A. A. Mostofi, J. R. Yates, I. Souza, and D. Vanderbilt, *Rev. Mod. Phys.* **84**, 1419 (2012).
- [57] A. A. Mostofi, J. R. Yates, Y.-S. Lee, I. Souza, D. Vanderbilt, and N. Marzari, *Computer Physics Communications* **178**, 685 (2008).
- [58] J. E. Hirsch, *Phys. Rev. B* **31**, 4403 (1985).
- [59] Y. Yanase, T. Jujo, T. Nomura, H. Ikeda, T. Hotta, and K. Yamada, *Physics Reports* **387**, 1 (2003).
- [60] S. Graser, T. A. Maier, P. J. Hirschfeld, and D. J. Scalapino, *New Journal of Physics* **11**, 025016 (2009).

- [61] D. J. Scalapino, *Rev. Mod. Phys.* **84**, 1383 (2012).
- [62] X. Wu, D. Di Sante, T. Schwemmer, W. Hanke, H. Y. Hwang, S. Raghu, and R. Thomale, *Phys. Rev. B* **101**, 060504 (2020).
- [63] M. C. Payne, M. P. Teter, D. C. Allan, T. A. Arias, and J. D. Joannopoulos, *Rev. Mod. Phys.* **64**, 1045 (1992).
- [64] G. Kresse and J. Furthmüller, *Phys. Rev. B* **54**, 11169 (1996).
- [65] H. Chen, A. Hampel, J. Karp, F. Lechermann, and A. J. Millis, *Frontiers in Physics* **10** (2022).